Astron. Astrophys. 333, 369–373 (1998)

ASTRONOMY AND ASTROPHYSICS

# Spatial differences in the visible/near infrared continuum emission of Comet C/1995 O1 (Hale-Bopp)

**Giancarlo Bellucci**

CNR Istituto di Fisica dello Spazio Interplanetario, Area di Ricerca di Tor Vergata, I-00133 Roma, Italy

Received 31 October 1997 / Accepted 27 November 1997

**Abstract.** Imaging spectroscopy data in the 0.4-1 $\mu$m spectral region of comet Hale-Bopp have been analysed in order to study the spatial distribution and physical properties of the dust grains in the coma. The data presented cover a period of three days close to perihelion. The spectra have been processed by means of the principal component analysis in order to individuate coherent spatial units with different spectral properties. The study shows the presence of two regions on the sunward and antisunward sides of the nucleus exhibiting different continuum emissions. This fact is interpreted as due to the presence of dust grains of diverse compositions and/or sizes. In the latter hypothesis, the observations could be explained by size sorting due to solar radiation pressure.

**Key words:** comets: general – comets: individual: C/1995 O1 (Hale-Bopp) – solar system: formation – techniques: spectroscopic

## 1. Introduction

Imaging spectroscopy is a powerful tool for the studying of planetary bodies. This technique provides the spectrum of each point in the scene, the so-called image cube (Vane et al. 1993). Since the spectrum contains direct information on the mineralogy and composition of the body, image cubes analysis allows the study of spatial distribution of mineral constituents present in the observed object. A drawback of this technique is the long observation time necessary to have good signal-to-noise ratio data. An imaging spectrometer, in fact, produces images in several narrow spectral bands ($> 100$), thus requiring either high light fluxes or long exposures. The situation is then more difficult in case of comets, which are normally faint objects. Comet Hale-Bopp (C/1995 O1) has provided the opportunity to observe a very bright comet. In this paper we present image cubes of comet Hale-Bopp taken in the 0.4-1 $\mu$m spectral range. The signal-to-noise ratio of the data allows a restricted part of the coma to be investigated. In our study we concentrate mostly on the spatial distribution of the dust continuum emission. The gas emission features are not discussed here in depth and will be the subject of a separate paper.

*Send offprint requests to*: G. Bellucci

## 2. Instrumentation and observations

We observed Hale-Bopp by using an imaging spectrometer in the 0.4-1 $\mu$m spectral range on the 1.5 m telescope at Sierra Nevada Observatory, Granada (Spain), on 20-24 March 1997. The comet was at a heliocentric distance $r_h$= 0.94 AU and a geocentric distance $\Delta$ = 1.32 AU. The phase angle was 49.1°. The spectrometer used a Thomson CCD detector, 384×288 pixels, of 23×23$\mu$m size, cooled by liquid nitrogen at -40 °C. The telescope was configured at $f/8$, yielding a scale of 0.4 arcsec per pixel. In order to increase the signal-to-noise ratio, the readout electronics allows selection of different operation modes by summing pixels on chip. We have used two modes by binning 2 or 3 pixels spatially and 2 spectrally, giving 0.8 or 1.2 arcsec per pixel along the slit and $\Delta\lambda$ = 50 Å, respectively. The images were obtained by acquiring the slit image at all wavelengths during the right ascension movement of the comet ($\approx$ 0.007 arcsec/sec). This produced images with different spatial scales, depending upon the selected instrument operation mode and exposure time. The images were also affected by geometrical distorsion, due to the fact that the angular resolution along slit was fixed and determined by the pixel size (0.8 or 1.2 arcsec) while across slit it was determined by the comet velocity and the exposure time (see Table 1). Details on the instrumentation are found in Bellucci et al. (1997). Here we will discuss only the image cubes taken on March 20 at 18:44 U.T. and March 22 at 18:43 U.T.; the reduction of the other images is still in progress and the results will be presented in the future. Relevant data set information is reported in Table 1. The data cubes consist of 144 monochromatic (bandpass $\Delta\lambda$ = 50 Å) images with different angular resolutions (1 arcsec = 970 km).

The slit was oriented N-S during the observations. Spectra were bias-subtracted and flatfielded corrected following standard procedures. A preliminary reduction for removing instrumental and atmospheric features from the comet spectrum has been done by dividing the spectra to that of a standard area named MS2 and located in Mare Serenitatis on the Moon (18°40′N 21°25′E, McCord et al. 1972). The normalised spectra reasonably approximate the spectral reflectivity of the coma,

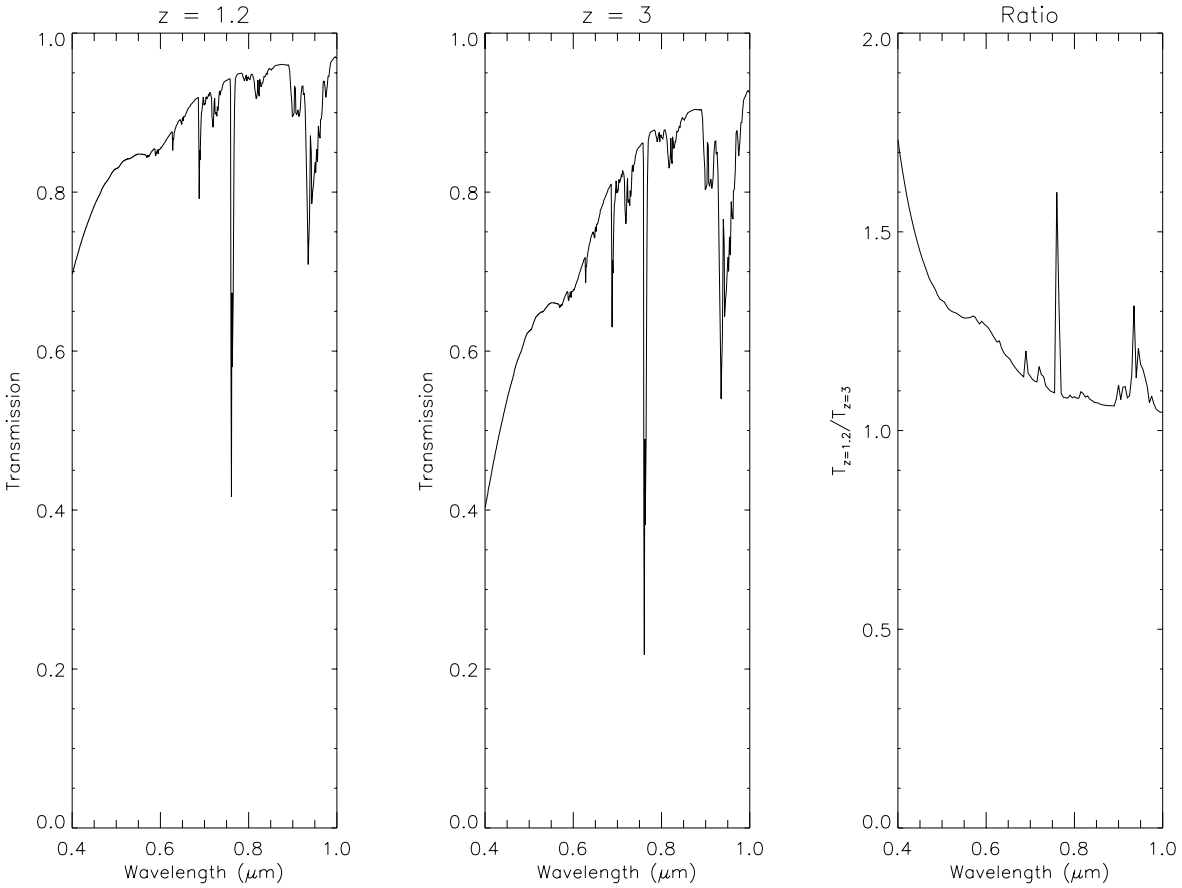


**Fig. 1.** Left and center panels: Transmission of the Earth atmosphere as computed using the LOWTRAN radiative transfer code at airmasses $z = 1.2$ and $z = 3$. Right panel: Ratio between $T_{z=1.2}$ and $T_{z=3}$.

**Table 1.** Summary of the observations

| Date | Time (U.T.) | Exposure time (sec) | Cube format (samples×lines×bands) | $\Delta\lambda$ (Å) | Angular resolution (H × V arcsec) |
|---|---|---|---|---|---|
| 20/03/97 | 0406 | 6 | 256×129×144 | 50 | 1.2×0.042 |
| 20/03/97 | 1807 | 20 | 384×027×144 | 50 | 0.8×0.22 |
| 20/03/97 | 1844 | 40 | 132×026×144 | 50 | 0.4×0.14 |
| 21/03/97 | 0430 | 31 | 192×022×144 | 50 | 0.8×0.22 |
| 22/03/97 | 1843 | 31 | 192×021×144 | 50 | 1.2×0.28 |

$S(\lambda)$, defined as the percentage of solar light scattered by the dust grains. However, due to the different airmasses of the comet ($z$ = 3) and the Moon (z = 1.2), the telluric features are not completely eliminated. We have attempted to correct the atmospheric extintion by using a radiative transfer computation (LOWTRAN, Kneitzys et al. 1983). Fig.1 shows (left and center panel) the fraction of solar light transmitted through the Earth atmosphere and computed at two different airmasses. On the right panel their ratio is shown. The reflectivity has then been computed by means of the following relation:

$$S(\lambda) = \frac{I_{HB}(\lambda)}{I_{MS2}(\lambda)} \times \frac{T_{z=1.2}(\lambda)}{T_{z=3}(\lambda)} \times S_{MS2}(\lambda) \quad (1)$$

where $I_{HB}(\lambda)$ and $I_{MS2}(\lambda)$ are the spectra of Hale-Boop and MS2, $T_z(\lambda)$ is the atmosphere transmission at $z = 1.2$ and $z = 3$, $S_{MS2}(\lambda)$ is the reflectivity of MS2 (McCord et al. 1972). The calculations made using the LOWTRAN code should be taken to provide a crude estimation of the decrease of radiant intensity through the atmosphere. This because the code uses average atmospheric profiles of the molecular species and aereosols which can be slightly different from a local situation. However, since we are interested to relative colour differences between portions of the image, residual atmospheric features do not constitute a serious problem. Curvature of spectra caused by atmospheric refraction has been corrected with an appropriate geometrical transformation (Bellucci et al. 1997).

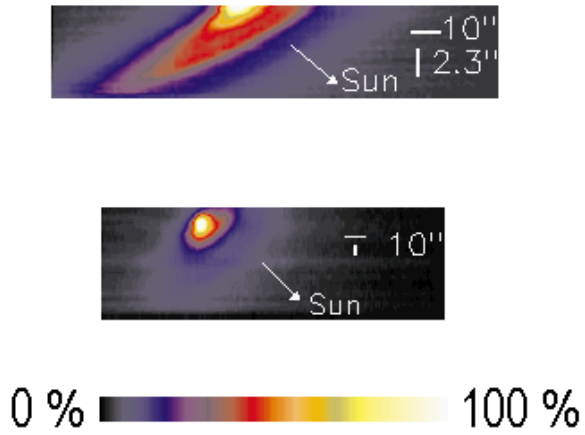


**Fig. 2.** Images at 0.7 $\mu$m of comet Hale-Bopp. North is on the left, East is up. The sun is in the S-W direction. Images taken on 20/03 at 18.44 U.T. (top) and 22/03 at 18.43 U.T. (bottom). The horizontal and vertical spatial scales are indicated ($1''$ = 970 km). The colour levels indicate intensity values relative to the peak of maximum brightness.

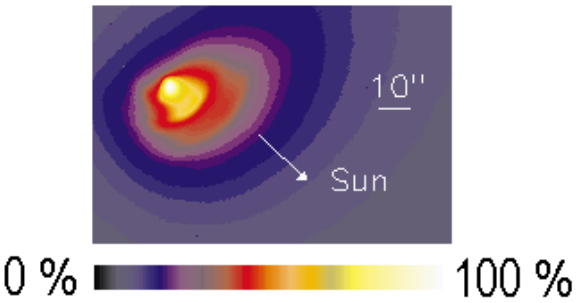


**Fig. 3.** CCD image in the R Johnson filter taken on 20/03 19.00 U.T. at the Loiano Observatory (Italy). The spatial scale is indicated in arcsec.

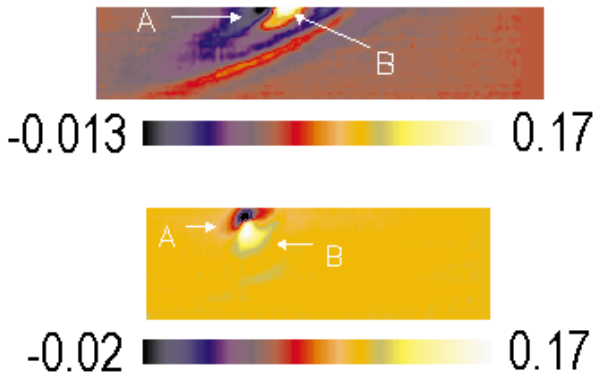


**Fig. 4.** Second principal components of image cubes discussed in the text. The arrows show regions whose spectra have different continuum emission. White-yellow colours indicate pixels with a continuum emission redder than those blue-black colored.

## 3. Data analysis and results

Due to lack of observing time the image cubes exposure was relatively short. This forced the subsequent analysis to a restricted part of the coma of about $30\times30\times10^3$ km. The signal-to-noise ratio in this region is about 40 for the brighter pixels at $\lambda$ = 0.7 $\mu$m and 15 at $\lambda$ = 0.4 $\mu$m. Fig. 2 shows the images at 0.7 $\mu$m of Hale-Bopp taken on 20/03 (top) and 22/03 (bottom), respectively. Although the images cover roughly the same portion of the coma, a comparison between them is made difficult by the diverse spatial scales and distorsions of the images. Moreover, the comet is not centered in the field due to pointing difficulties.

For comparison purpose, an undistorted CCD image of the comet in the Johnson red filter is shown in Fig.3 . It was taken at the Loiano Observatory (Italy) on 20/03 19.00 U.T..

An arc structure is visible in the sunward direction. In order to study possible colour variations occurring in the coma and connected to the physical properties of the grains, we have processed the two image cubes by means of the principal component analysis (PCA in the following, Davis 1986; Erard et al. 1991; Bell 1992; Chevrel et al. 1994). This is a common technique generally used to study the spectral content of image cubes and to individuate coherent spatial units exhibiting an extreme spectral behaviour. It uses a linear transformation of the data to translate and rotate them in a new coordinate system that maximizes the variance. After this transformation, the new components are statistically independent and the information is contained in few principal component (henceforth PC) images while most of the noise is segregated in the other components. Mathematically, the PCA involves the calculation of the eigenvectors of the variance-covariance matrix of the data and then the transformation of the data into a set of orthogonal axes that are a linear combination of the original data. The first transformed image normally depicts the average brightness of the coma while the other components contain the colour information and are generally pairwise differences between the original spectral channels. In Table 2 the relevant statistic for 3 components is reported. Eigenvalues for bands that contain information are an order of magnitude larger than those that contain only noise. The corresponding images are spatially coherent, while the noise images do not contain any spatial information.

Spectral channels from 0.4-0.5 $\mu$m were excluded to avoid the $C_2$ emission features. The first principal component images are albedo pictures and are similar to the images shown in Fig.2. In fact, brightness is the first cause of pixel spectral diversity within each image cube. The second PC images are shown in Fig. 4. The regions indicated by arrows (A and B) exhibit different spectra. These two regions are roughly the same in the two images and correspond to the antisunward and sunward directions, respectively.

Here, the spectral difference is linked mainly to the continuum emission, which is the second cause of pixel spectral variability within each image cube. Representative reflectivity spectra (samples from image cube 20/03 18.44 U.T.) of the regions labelled A and B are shown in Fig. 5. The reflectivities are normalized to 5 800 Å. Region B spectra have a rate of increase of the reflectivity $\left(\frac{dS}{d\lambda}\right)$ greater than the region A spectra. In order to compare the reflectivity gradient to that of other comets, we have followed the method illustrated in Jewitt and Meech (1986b), defining the normalized reflectivity gradient between wavelength $\lambda_1$ and $\lambda_2$, $S'(\lambda_1,\lambda_2) = \left(\frac{dS}{d\lambda}\right)/S_{mean}$.

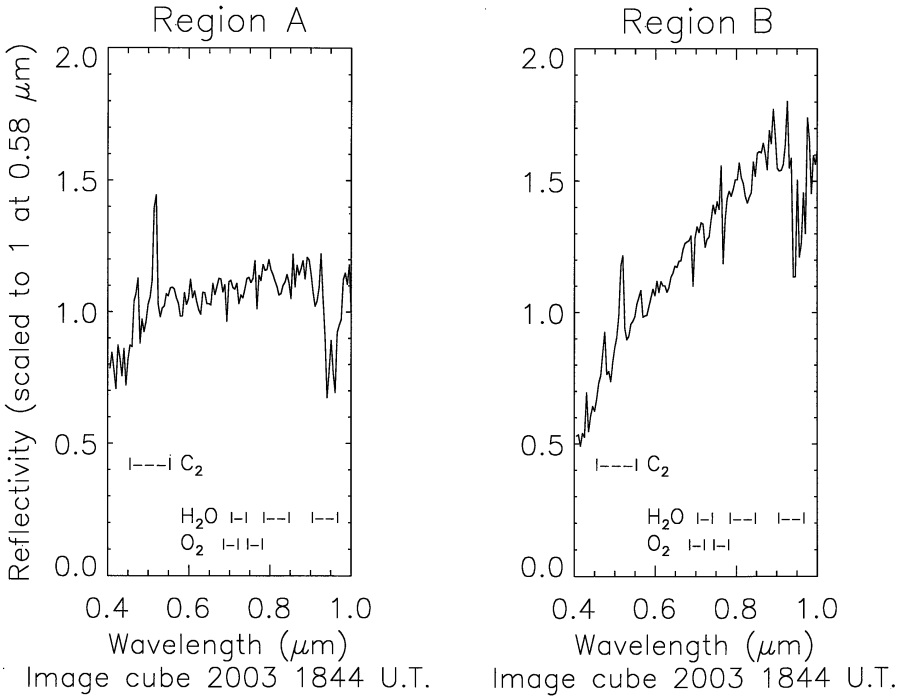


**Fig. 5.** Reflectivity of regions indicated by arrows in the PC images of Fig. 4. Main telluric absorption features are indicated. The reflectivity has been normalized at 5 800 Å.

**Table 2.** Relevant statistics of three principal components. The units are in digital numbers.

Image cube 20/03/97 18:44 U.T.

| PC image | Min | Max | Mean | Stdev | Eigenval |
|---|---|---|---|---|---|
| 1 | -0.0098 | 0.1619 | 0.0121 | 0.0158 | 0.0188 |
| 2 | -0.0129 | 0.1681 | 0.0122 | 0.0152 | 0.0002 |
| 3 | -0.0081 | 0.1618 | 0.0115 | 0.0149 | 0.0000 |

Image cube 22/03/97 18:43 U.T.

| PC image | Min | Max | Mean | Stdev | Eigenval |
|---|---|---|---|---|---|
| 1 | -0.0192 | 0.1580 | 0.0072 | 0.0128 | 0.0152 |
| 2 | -0.0192 | 0.1676 | 0.0082 | 0.0132 | 0.0003 |
| 3 | -0.0179 | 0.1534 | 0.0073 | 0.0122 | 0.0001 |

Here $dS/d\lambda$ is computed in the interval $\lambda_1$ to $\lambda_2$ and $S_{mean}$ is the mean reflectivity in the $\lambda_1$ - $\lambda_2$ wavelength range. In the optical, $S' \approx 18\%$ per 1000 Å (B region) and $\approx 5\%$ per 1000 Å (A region). These values are within the range defined by other comets (e.g. Levy-Rudenko, P/Halley and P/Shoemaker 1984S, Jewitt & Meech 1986b). Moreover, the spectra of region A exhibit reflectivity values in the 0.4-0.5$\mu$m range higher than the respective region B spectra. This fact cannot be attributed to the airmass variation within the image cube. Actually, a systematic increasing of spectral slope with airmass does not exist. Moreover, the previous argumentation excludes also atmospheric refraction of the spectra to be the cause of the observed phenomenon. We do not exclude, however, that minor residual effects could still plague the data. Anyway, the absence of systematic trends of spectral redness in the pixels of regions A and B, rules out the possible instrumental nature of the effect shown in Figs. 4 and 5. The blue excess seen in the region A spectra could be also due to the rather strong $C_2$ gas emission present in this wavelength interval. However, the excess still remains at the continuum wavelengths, such as 4450 Å and 5260 Å.

## 4. Discussion

The results shown above suggest the presence in coma of comet Hale-Bopp of discrete regions where grains with different size and/or composition are present. Spatial gradients in the continuum emission of a comet coma have been firstly reported by Jewitt & Meech (1986a). They showed that the grain continuum on the sunward side of the nucleus of comet P/Halley was redder than on the antisunward side. The same effect is shown in Fig. 4 and 5. The authors attributed these variations to particle size sorting by solar radiation pressure. Although a comprehensive model of the observations would require knowledge of size distribution, complex index of refraction, structure and shape of the particles (data not fully determined), some qualitative constrains on the nature of the grains can be placed, in the light of the already available data. The wavelength dependence of the intensity of solar light scattered by the grains, $I(\lambda)_{sca}$ , is proportional (neglecting phase dependence effects and considering an optically thin coma) to the efficiency factor for scattering of the particles, $Q(\lambda)_{sca}$ . When the particles are very much larger than the wavelength (Mie size parameter $x = 2\pi a/\lambda >> 1$ where $a$ is the particle radius), $Q_{sca}$ becomes independent of wavelength. If grains in regions A, B have the same composition but different sizes, spectra plotted in Fig. 5 indicate that $x >\approx 1$. This implies the presence of particles having different size, likely in the $0.1 < a < 1\mu$m interval. On the contrary, if $I_{sca}$ wavelength dependence is the result of the compositional, rather than size effects, region A spectra could be fitted by particles scattering more efficiently than silicate grains (region B) at shorter wavelengths, such as icy or carbonaceous particles.

Several pieces of evidence can be interpreted in terms of the size and composition of dust grains. The intensity of thermal emission in the 8 - 13 $\mu$m range indicates the presence of small ($<1$ $\mu$m) grains in the inner coma (Hayward & Hanner, 1997). The authors suggest also that much of this fine material originates from localised active areas on the nucleus. The strong silicate emission at 11.2 $\mu$m (Crovisier et al. 1996, 1997) has been found consistent with Mg-rich crystalline olivine (forsterite), maybe in the form of sub-micrometric grains (Colangeli et al 1995). Larger grains ($<5$ $\mu$m) are also suggested (Lisse et al. 1997) to explain infrared observation of the dust. $H_2O$ sublimation from icy grains has been seen when the comet was at large heliocentric distances (Davies et al. 1997; Biver et al. 1997). Additional organic components may also be present (Davies et al. 1997; Sarmecanic et al. 1997). A preliminary analysis of the $C_2$ ($\Delta\nu = 0$) emission feature, indicated in Fig. 5, shows a spatial correlation with the distribution of dust. This fact strengthens the organic nature of dust grains.

*Acknowledgements.* The author wishes to thank the support staff and telescope operators of the Sierra Nevada and Loiano Observatories. Without their help the observations would not have been possible. He specially thanks Dr. M. Herranz de la Revilla and Dr. J. L. Moreno of the Institute of Astrophysics of Andalucia for their continuous assistance. The author is also grateful to Prof. V. Formisano for helpful discussion and to Mrs. S. Zampieri for her support during the manuscript preparation. Fundings were provided by ASI and CSIC grants.

## References

Bell J.F., 1992, Icarus, 100, 575.
Bellucci G. et al., 1997, Planetary Space Science, in press.
Biver N., Bockelée-Morvan D., Colom P. et al., 1997, Science 275, 1915.
Chevrel S. et al., 1994, Lunar Planetary Sci., Conf. 25th, Part 1, 249.
Colangeli L., Mennella V., Di Martino C. et al., 1995, A&A 293, 927.
Crovisier J., Brooke T.Y., Hanner M. S. et al., 1996, A&A 315, L385.
Crovisier J., Leech K., Bockelée-Morvan D. et al., 1997, Science 275, 1904.
Davis J.C., 1986, in: Geology, Wiley (ed.), New York.
Davies J.K., Roush T.L., Cruikshank D.P. et al., 1997, Icarus 127, 238.
Vane G. et al., 1993, in: Pieters C.M. and Englert P.A.J. (eds.), Remote Geochemical Analysis: Elemental and Mineralogical Composition, p.215
Erard S., Bibring J.P., Mustard J. et al., 1991, Proc. Lunar Planet. Sci. Conf. 21th, Vol.21, 437.
Hayward T. L., Hanner M. S., 1997, Science 275, 1907.
Jewitt D. C., Meech K. J., 1986a, Proc. 20th Eslab Symposium, Vol.2, 47.
Jewitt D. C., Meech K. J., 1986b, Astrophysical Journal, 310, 937-952.
Kneitzys F.X., Shettle E.P., Gallery W.O. et al., 1983, Environmental Research Papers, No.846.
Lisse C. M., Fernández Y.R., A'Hearn M.F. et al., 1997, BAAS 29,1004.
McCord T. B., Charette M.P., Johnson T. V. et al., 1972, JGR 77, 1349.
Sarmecanic J. R., Osip D. J., Lederer S. M. et al., 1997, BAAS 29,1004.